Journal Name

COMMUNICATION

Surface recombination velocity of $CH_3NH_3PbBr_3$ ~~perovskite~~ nanowires in anodic aluminium oxide templates

Received 00th January 20xx,
Accepted 00th January 20xx

DOI: 10.1039/x0xx00000x

www.rsc.org/

Parisa Khoram,[a,‡] Sebastian Z. Oener, [a,b,‡] Qianpeng Zhang,[c] Zhiyong Fan,[c] and Erik C. Garnett*[a]

Here we present successful surface passivation of halide perovskite nanowires with anodic aluminum oxide templates. The $CH_3NH_3PbBr_3$/alumina nanowires have charge carrier lifetimes of more than 20 ns and a remarkably low surface recombination velocity of 37.2±20 cm/s. Ease of fabrication and excellent photophysical properties make them a promising candidate for integration in optoelectronic device structures.

Shockley-Read-Hall (SRH) surface and bulk recombination is detrimental for the performance of semiconductor-based devices, especially at low charge carrier injection levels.[1] Thus, for high-efficiency devices, strategies mitigating the influence of those defects must be developed, with varying requirements for bulk and surface defects. Hybrid halide perovskites are not an exception to this rule, as their efficient performance is tightly bound to tackling the right approaches for identifying and confronting their defects. Their unusual defect chemistry and physics has enabled the rapid and simple fabrication of high quality absorbers and emitters with long charge-carrier diffusion lengths and lifetimes, high absorption coefficients and high emission yields.[2–4] Those photo-physical properties in turn depend directly on the charge carrier generation and recombination dynamics. Thus, it is crucial to provide in-depth understanding of how fast and via which channels the charge carriers recombine within the perovskite light-absorber. This knowledge assists in developing strategies to minimize the structural imperfections, such as bulk and surface lattice defects for designing highly efficient optoelectronic devices. Interfacial defects facilitate the charge recombination processes and impact the overall performance of the device negatively.[5]

Passivating the surfaces of traditional inorganic semiconductors such as Si was a milestone in achieving highly efficient solar cells.[6] In halide perovskites, similar passivation methods have been investigated by incorporation of external materials as well as new approaches according to their special chemical structure, such as self-formation of PbI_2 on $CH_3NH_3I_3$ thin films through ambient exposure.[7–9] Surfaces, interfaces or grain boundaries of halide perovskites have been passivated using chemical treatments via halogenated organic compounds,[10] Lewis bases,[11] fullerene,[12–15] graphene[16] and potassium.[17] Many research groups investigated the application of ultra-thin metal oxide films, such as ZnO,[18–21] SnO_x [20] and Al_2O_3 [19,21–26] by atomic layer deposition (ALD) as passivation layers in halide perovskite solar cells. Note that this is different than the common use of ALD metal oxides as the carrier-selective charge transfer layers in planar perovskite solar cells.[27] In most of the surface passivation studies, the addition of an oxide layer improved device performance and stability. However, little is known about the charge carrier dynamics at the perovskite/metal oxide interfaces and in particular the recombination rates and SRV have not been quantified at these interfaces.

Nanowires are promising geometries for applications in electronic and optoelectronic devices[28–30] and also for case studies of dimension-dependent properties. Previously, semiconductor nanowires such as Ge,[31] Si[32,33] and InP[34] were studied to quantify the dynamics of charge carriers and/or investigate the effects of surface passivation. By controlling their surface to volume ratio, they provide a versatile platform to manage and quantify the contribution of surface and bulk precisely. In the past few years, perovskite nanowires have been realized via various solution[35] and vapour-based methods.[36,37] Among those, perovskite nanowires embedded in anodic aluminum oxide (AAO) templates have been successfully incorporated in efficient solar cells[38] and photodetector devices[39,40], demonstrating the high potential of perovskite nanowires wrapped with alumina (perovskite/alumina) for future applications.

[a] Center for Nanophotovoltaics, AMOLF, Science Park 104, 1098 XG Amsterdam, The Netherlands
[b] Department of Chemistry and Biochemistry, University of Oregon, Eugene, Oregon 97403, USA.
[c] Department of Electronic and Computer Engineering, The Hong Kong University of Science and Technology, Clear Water Bay, Kowloon, Hong Kong SAR, China
‡ These authors contributed equally.

Electronic Supplementary Information (ESI) available: [details of any supplementary information available should be included here]. See DOI: 10.1039/x0xx00000x

Here we study the recombination dynamics at the perovskite/alumina interface using perovskite nanowires embedded in anodic aluminum oxide (AAO) templates. The nanowires are fabricated by applying a pressure gradient across a template coated with a viscous halide perovskite precursor solution, similar to the extrusion technique we introduced previously.[41] Fabrication from perovskite solution directly into the AAO template avoids the exposure of the water-sensitive perovskite surface to the water precursor in a typical Al_2O_3-ALD process. By using templates with various pore sizes from ~150 to ~350 nm, we systematically change the surface to volume ratio of the final $CH_3NH_3PbBr_3$ perovskite nanowires. Assuming the bulk quality and radiative rates stay constant, the changes in total recombination rates should be directly connected to the recombination at the perovskite nanowire surfaces. Time-resolved PL (TRPL) spectroscopy is used to obtain the dynamics of photoexcited carriers in the perovskite nanowire arrays. The recombination rates are extracted by fitting the PL intensity decay to a rate equation that includes radiative and non-radiative recombination. The obtained lifetime increases slightly from 24.3±2.3 ns to 28.3±1.5 ns when increasing the diameter by more than a factor of two. This shows the weak dependence of PL lifetime on nanowire diameter, suggesting a very low surface recombination velocity (SRV). By fitting these TRPL results to a simple recombination model, we extract an SRV of 37.2±20 cm/s, indeed much lower than the value measured for unpassivated surfaces of single crystal $CH_3NH_3PbBr_3$ perovskites (~10^3 cm/s)[42–44]. These results indicate that alumina provides excellent passivation for $CH_3NH_3PbBr_3$ perovskite nanowires. This structure can be extended to incorporation into future devices.[38–40]

To fabricate the perovskite/alumina nanowires, we employed a differential-pressure-driven process similar to the extrusion method introduced previously[41]. However, when the perovskite solution inside the AAO pores reaches the AAO top surface the process is terminated (before nanowire extrusion), as schematically shown in Figure 1a. The perovskite solution fills the nanopores of the AAO template and evaporation of the solvent leaves perovskite/alumina nanowires inside the AAO pores. Figure 1b shows the SEM images from the bottom surface of the template prior to filling with perovskite, whereas SEM image in Figure 1c indicates the filling of the pores after the application of a pressure gradient. Conductivity measurements (Figure S1) and cross-sectional SEM images (Figure S2) of filled AAO templates show that the perovskite is extended through a large fraction of the AAO pores (see SI). This simple method provides highly ordered arrays of perovskite nanowires with tuneable lengths (determined by the AAO thickness) embedded in a transparent medium with high surface passivation potential.

The optical properties of the perovskite/alumina nanowires are characterized with steady-state PL (405 nm excitation) and absorption measurements (Figure 2a). The emission peak at 540 nm (2.29 eV) matches the band gap of $CH_3NH_3PbBr_3$. The nanowire arrays with different diameters, but the same length (50 µm), have similar PL and absorption spectra. Finite-difference time-domain (FDTD) simulations are performed to

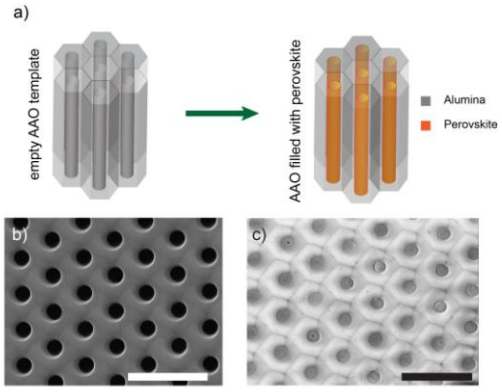

Figure 1. $CH_3NH_3PbBr_3$ nanowires embedded in AAO template. a) Schematic of AAO template before and after filling with perovskite solution. b) SEM image of the bottom side of the template before and c) after the pores were filled with the solution. The scale bars correspond to 2 µm.

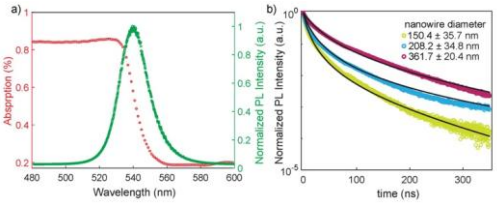

Figure 2. Steady-state PL, absorption and transient PL of perovskite/alumina nanowire arrays. a) PL (405 nm excitation) and absorption spectra of the nanowire arrays with average diameter 361.7 nm. The samples with smaller diameter had similar absorption and PL spectra as shown in the SI. b) PL intensity decay of nanowire arrays with various diameters. The black line shows the fit to the data according to Equation 3.

study the light intensity distribution and absorption in perovskite/alumina nanowire arrays with various diameter, as presented in Figure S3. The electric-field intensity ($|E|^2$) upon the excitation with short-wavelength light (485 nm) decays quickly within the first 5 nanometers away from the surface for all the nanowire arrays with different diameters. The simulated absorption spectrum is in agreement with the experimental absorption data shown in Figure 2a.

We used three templates with average pore diameters of 150.4±35.7, 208.2±34.8 and 361.7±20.4 nm and filled them with $CH_3NH_3PbBr_3$ nanowires to study the charge carrier dynamics and the contribution of the perovskite/alumina interface in the recombination mechanism. By decreasing the nanowire diameter and keeping the bulk recombination constant, we increase the relative contribution of the surface to the overall recombination process. Since all the samples were prepared from the same solution batch at the same time, and also measured at the same time, we expect the bulk quality and defect densities to be comparable for all of them. Therefore, changing nanowire diameters would affect the non-radiative recombination because of the higher density of trap states on the surface. Here we assume that there is no

radiative channel in trap-assisted recombination and the only radiative process leading to emission is bimolecular recombination of two charge carriers.[45] Therefore the decay of PL as a function of time can be written as:

$$PL(t) = Ak_2 n(t)^2 + bcg \quad (1)$$

Where *A* is the collection efficiency, *n(t)* is the charge carrier density as a function of time and *bcg* is the background. Here, k_2 is the bimolecular recombination rate coefficient defined *via* the decay of charge carriers over time, as formulated below:

$$\frac{dn(t)}{dt} = -k_3 n(t)^3 - k_2 n(t)^2 - k_1 n(t) \quad (2)$$

Where k_1 is the recombination rate coefficient associated with the monomolecular trap-assisted recombination and k_3 is the Auger recombination rate coefficient.

We measured *PL(t)* of the nanowire arrays with time-correlated single photon counting (TCSPC) over more than 8 different spot on each sample (details in SI). A blue laser (485 nm) with a fluence of 8.3 μJ.cm^{-2} excited the samples and generated an initial charge carrier density of 3.2x10^{17} cm^{-3}. The calculation of carrier density is explained in detail in the SI. At this carrier density, the role of Auger recombination is considered negligible.[45,46] The representative PL decay curves of each sample are shown in Figure 2b. We solved Equation 2 for *n(t)*, disregarding the Auger term, and inserted the result in Equation 1:

$$PL(t) = Ak_2\left(\frac{k_1 n_0}{(k_1 + k_2 n_0)\exp(k_1 t) - k_2 n_0}\right)^2 + bcg \quad (3)$$

Where n_0 is the initial carrier density at *t=0* and k_1 is the trap-assisted recombination coefficient.

Globally fitting Equation 3 to the experimental TRPL data allows us to extract the trap-assisted and radiative recombination coefficients k_1 and k_2 as listed in Table 1. More details of the fitting procedure can be found in the SI.

Table 1. Recombination coefficients of $CH_3NH_3PbBr_3$/alumina nanowires with different diameters extracted from global fitting of Equation 3 to measured PL decay, as shown in Figure 2b. The average diameter of the nanowire (d) was measured *via* SEM over ~40 nanowires for each sample. The errors are standard deviations. Here, k_1 is the trap-assisted recombination coefficient and k_2 is the radiative recombination coefficient. The errors are standard errors of the mean of the extracted coefficients measured over more than 8 different spot for each sample. The charge carrier lifetime τ is calculated from equation 4 and the errors are standard error of the means.

d (nm)	k_1 (x10^6 s^{-1})	k_2 (x10^{-10} cm^3 s^{-1})	τ (ns)
150.4±35.7	3.71±0.58	1.32±0.24	24.3±2.3
208.2±34.8	3.99±0.92	1.31±0.19	26.9±3.5
362.7±20.4	2.10±0.29	1.06±0.06	28.3±1.5

As seen in Table 1, increasing the nanowire diameter enhances the lifetime of charge carriers. The changes in k_1 can be attributed to the changes of surface defect density due to different surface contribution of each nanowire array, as well as sample-to-sample bulk defect density variations. Nevertheless, the decrease in k_1 follows a trend with increasing nanowires diameter considering the error bars of the experiment. The variation of k_2 from sample to sample is small, confirming that the radiative processes come from the band-to-band recombination and therefore depend on the materials' band structure and local density of states. The k_1 values are in the same range as measured by Richter et al.[47] with Transient Absorption (TA) for $CH_3NH_3PbBr_3$ thin films (2.5x10^6 s^{-1}) and by Wu et al.[44] for $CH_3NH_3PbBr_3$ single crystals with TRPL (2.9x10^6 s^{-1}), but one order of magnitude lower than values reported by Yang et al.[46] from TA measurements (2.7x10^7 s^{-1}) for $CH_3NH_3PbBr_3$ thin films. The radiative recombination coefficient is also comparable to the studies by Wu et al.[44] and Yang et al.[46], but ~10 times lower than reference Richter et al.[47] Using the recombination coefficients, we calculated the charge carrier lifetime from Equation 4 as presented in the last column of Table 1.

$$\tau = \frac{1}{k_1 + k_2 n} \quad (4)$$

The lifetime is relatively stable, increasing only slightly with diameter. Thus the relative surface contribution to the overall charge carrier recombination is small for the high surface passivation levels obtained here.

In the long nanowires studied here, the diameter is essentially the identifier of surface area to bulk volume. In order to discover the exact dependence of the recombination on the surface, we developed a model to relate the carrier lifetime to the nanowire diameter.

In the following, we assume a charge carrier diffusion length in $CH_3NH_3PbBr_3$ that is larger than the radius of the nanowires[25] and hence a homogenous carrier concentration inside each individual nanowire and among all nanowires inside the laser spot. In this model, the surface recombination velocity is essentially a rate parameter that, together with bulk recombination, reduces the photo-generated carrier concentration observed via PL. Specific carrier gradients inside the nanowire, leading to complex carrier flow patterns are neglected. For a certain geometry, the total recombination is composed of two terms –bulk and surface– as shown below:

$$R_T = VR_B + AR_S \quad (5)$$

Where R_T is the total recombination rate, *V* is the volume, *A* is the surface area, and R_B and R_S are the total recombination rates in the bulk per unit volume and at the surface per unit area. Considering the geometry of the nanowire as a cylinder with radius *r* and length l the equation above can be written as:

$$R_T = \pi r^2 l(B + S_{air}/l) + 2\pi r(lS_{alumina}) \quad (6)$$

Where B is the bulk recombination velocity, $S_{alumina}$ and S_{air} are the rate at which the charge carrier move towards the nanowire interfaces (SRV) with alumina and air respectively. Since B and S_{air} have the same dependence on the radius, we group them together as an effective bulk recombination term (R_v). By dividing both sides of Equation 5 by $\pi r^2 l$ (the nanowire volume), we end up with Equation 7, which allows

us to extract $S_{alumina}$ from the slope of the recombination rate versus inverse of the nanowire radius:

$$R = R_v + \frac{2S}{r} \quad (6\text{-}7)$$

where R is the recombination rate per unit volume given by $R(n,t) = k_2 n + k_1$ and by definition is the inverse of charge carrier lifetime (1/τ). Therefore, Equation 6-7 is rearranged in the final form:

$$\frac{1}{\tau} = R_v + \frac{2S}{r} \quad (7\text{-}8)$$

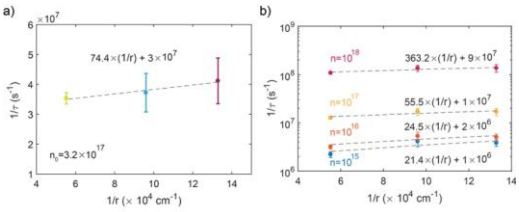

Figure 3. Modeling the surface recombination velocity (SRV) of perovskite/alumina using nanowires with various diameters. a) Recombination rate (1/τ) versus inverse of nanowire radii. The lifetime is calculated from Equation 4 for the initial carrier density as performed in the TRPL experiment. The dashed line shows the linear fit of Equation 8 to the experimental data. The equation achieved from the fit is written above the line. The slope is equal to 2*SRV and the y-intercept is effective bulk recombination. b) The estimation of SRV and total bulk recombination for various carrier densities from 10^{15} to 10^{18} cm^{-3}. With increasing carrier density SRV increases, but the effective bulk recombination stays dominant.

The inverse of the carrier lifetime is proportional to the inverse of nanowire radius, where the slope of the line is 2S, and y-intercept is the effective bulk recombination rate. This model shows that the lower the slope is, the less the nanowire wall surface contributes to the recombination rate. Therefore if a perfect passivation of the surface is provided, the line would be horizontal with slope zero, and recombination stemming only from the bulk and top surface. A similar approach using the continuity equation was implemented before by Leonard et al.[31] and Dan et al.[33] and the same linear relation of the recombination rate and nanowire diameter was derived, as also explained in SI.

Fitting Equation 7-8 to the inverse of the average lifetimes (calculated from Equation 4 for more than 8 experiments for each sample) versus the inverse of nanowire radius results in an SRV of 37.2±20 cm/s and bulk recombination rate of $3x10^7$ s^{-1} at the initial carrier density of $3.2x10^{17}$ cm^{-3} (Figure 3a). The error is the standard deviation of SRV extracted from 10^6 linear fits of the averages of 5 randomly selected data points at each nanowire radius. This result shows that at this carrier density, the recombination is dominated by the bulk (with possible contributions from the top surface), and the side wall surface is well passivated. This value is considerably lower than SRVs reported in the various studies for the unpassivated $CH_3NH_3PbBr_3$ single crystals[43,44,48,49] (1.6-6.7x 10^3 cm/s) and lower but in the same range as reported for the passivated surface of $CH_3NH_3PbBr_3$ single crystals with UV-O_3 treatment (64 cm/s).[48] Fang et al.[50] reported an unusually low SRV of 4 cm/s for the $CH_3NH_3PbBr_3$ single crystals by controlling the physisorption of oxygen and water molecules on their surface.

We should note that SRV is a facet dependent parameter. While single crystals of $CH_3NH_3PbBr_3$ have (100) facets because of their cubic structure, the nanowire walls have higher index facets. Figure S3 shows the X-ray diffraction (XRD) pattern of the $CH_3NH_3PbBr_3$/AAO nanowires. The (100) diffraction peaks are pronounced which indicates that the nanowires within the AAO pores are grown in the <100> direction. In contrast, the nanowire side walls are higher index facets, such as (200), which are clearly visible in the XRD spectra, too. Most semiconductor nanowires, such as Si[33] and Ge,[31] have SRVs 2-3 orders of magnitude higher than what is reported in this study. Obtaining the incredibly small SRV values of 37.2±20 cm/s for high index facets of perovskite nanowires confirms the good passivation that alumina provides.

The SRV depends not only on surface trap states (their type and density), but also on the charge carrier density.[6] Therefore we expect an increase in SRV with increasing carrier density. We used the same recombination coefficients in Table 1, and plotted various total recombination lifetimes versus the nanowire radii in Figure 3b for charge carrier densities of 10^{15} - 10^{18} cm^{-3}. A higher carrier concentration is not selected because of the increasing contribution of Auger recombination with higher intensities[51], which is not included in our model. By fitting Equation 7-8 with the different carrier densities to the dependence of the lifetime on the nanowire radius, as shown in Figure 3b, we obtained the respective surface and effective bulk as summarized in Table 2. The last column of this table shows that increasing the carrier density effectively makes the contribution of surface recombination to the total recombination rate ($S/d + R_v$) smaller.

Table 2. Surface (S) and effective bulk (R_v) recombination velocities for $CH_3NH_3PbBr_3$ /alumina nanowires at different carrier densities. S and R_v are fit parameters as shown in Figure 3b. S/(R_v.d_{av}+S) is the contribution of surface recombination to the total recombination for a representative nanowire with average diameter of d_{av}=200 nm.

n (cm^{-3})	S (cm/s)	R_v (s^{-1})	S/(R_v.d_{av}+S) (%)
10^{15}	10.7	10^6	34.4
10^{16}	12.3	$2x10^6$	23.5
10^{17}	27.7	10^7	12.2
10^{18}	182.2	$9x10^7$	9.2

Conclusions

In this study we fabricated long $CH_3NH_3PbBr_3$ nanowire arrays embedded in AAO templates (perovskite/alumina nanowires) using a simple solution technique by suction of the perovskite solution through the AAO pores. The charge carrier recombination mechanism of the perovskite/alumina nanowire arrays was studied with time-resolved PL spectroscopy. Fitting of the PL intensity decay to a rate equation that includes radiative (bimolecular) and non-radiative (monomolecular) recombination was used to obtain the recombination rate coefficients. We estimated a charge

carrier lifetime of more than 20 ns at the initial carrier density of $3.2x10^{17}$ cm^{-3} for nanowires with various diameters. The inverse lifetimes increase linearly with decreasing nanowire diameter. This data was fitted to a model to extract a very low SRV of 37.2±20 cm/s at the $CH_3NH_3PbBr_3$/alumina interface. The low SRV of passivated nanowires in comparison to unpassivated $CH_3NH_3PbBr_3$ single crystals (~10^3 cm/s)[44,49,52] ensures that despite the large surface of perovskite nanowires, their surface was not dominant in recombination processes.

The presented results here confirm the passivation effect alumina provides for hybrid halide perovskites and quantifies the surface recombination velocity at the perovskite/alumina interface for the first time. This study presents a simple systematic method for the passivation of perovskite surfaces, without the need for ALD deposition of Al_2O_3. Further studies to compare the perovskite nanowires passivated with ALD and the ones embedded in AAO templates will provide a comprehensive picture of the similarities and differences of these two methods.

Conflicts of interest

There are no conflicts to declare.

Acknowledgements

This work was done at AMOLF and partially supported supported by the Netherlands Foundation for Scientific Research (NWO) as well as the European Research Council (Grant Agreement No. 337328). The work in The Hong Kong University of Science and Technology was supported by General Research Fund (project 16237816) from the Hong Kong Research Grant Council, and National Natural Science Foundation of China (project 51672231).

Notes and references

1 W. Shockley and W. T. Read, *Phys. Rev.*, 1952, **87**, 835–842.
2 M. a. Green, A. Ho-Baillie and H. J. Snaith, *Nat. Photonics*, 2014, **8**, 506–514.
3 S. D. Stranks and H. J. Snaith, *Nat. Nanotechnol.*, 2015, **10**, 391–402.
4 H. Wang and D. H. Kim, *Chem. Soc. Rev.*, 2017, **46**, 5204–5236.
5 J. Shi, X. Xu, D. Li and Q. Meng, *Small*.
6 A. G. Aberle, *Prog. Photovoltaics Res. Appl.*, 2000, **8**, 473–487.
7 L. Wang, C. McCleese, A. Kovalsky, Y. Zhao and C. Burda, *J. Am. Chem. Soc.*, 2014, **136**, 12205–12208.
8 Q. Chen, H. Zhou, T. Song, S. Luo and Z. Hong, *Nano Lett.*, 2014, **14**, 4158–4163.
9 T. J. Jacobsson, J.-P. Correa-Baena, E. Halvani Anaraki, B. Philippe, S. D. Stranks, M. E. F. Bouduban, W. Tress, K. Schenk, J. Teuscher, J.-E. Moser, H. Rensmo and A. Hagfeldt, *J. Am. Chem. Soc.*, 2016, **138**, 10331–10343.
10 A. Abate, M. Saliba, D. J. Hollman, S. D. Stranks, K. Wojciechowski, R. Avolio, G. Grancini, A. Petrozza and H. J. Snaith, *Nano Lett.*, 2014, **14**, 3247–3254.
11 N. K. Noel, A. Abate, S. D. Stranks, E. S. Parrott, V. M. Burlakov, A. Goriely and H. J. Snaith, *ACS Nano*, 2014, **8**, 9815–9821.
12 K. Wojciechowski, S. D. Stranks, A. Abate, G. Sadoughi, A. Sadhanala, N. Kopidakis, G. Rumbles, C.-Z. Li, R. H. Friend, A. K.-Y. Jen and H. J. Snaith, *ACS Nano*, 2014, **8**, 12701–12709.
13 J. Xu, A. Buin, A. H. Ip, W. Li, O. Voznyy, R. Comin, M. Yuan, S. Jeon, Z. Ning, J. J. McDowell, P. Kanjanaboos, J.-P. Sun, X. Lan, L. N. Quan, D. H. Kim, I. G. Hill, P. Maksymovych and E. H. Sargent, *Nat. Commun.*, 2015, **6**, 7081.
14 Y. Shao, Z. Xiao, C. Bi, Y. Yuan and J. Huang, *Nat. Commun.*, 2014, **5**, 5784.
15 J. Peng, Y. Wu, W. Ye, D. A. Jacobs, H. Shen, X. Fu, Y. Wan, T. Duong, N. Wu, C. Barugkin, H. T. Nguyen, D. Zhong, J. Li, T. Lu, Y. Liu, M. N. Lockrey, K. J. Weber, K. R. Catchpole and T. P. White, *Energy Environ. Sci.*, 2017, **10**, 1792–1800.
16 H. Li, L. Tao, F. Huang, Q. Sun, X. Zhao, J. Han, Y. Shen and M. Wang, *ACS Appl. Mater. Interfaces*, 2017, acsami.7b10773.
17 M. Abdi-Jalebi, Z. Andaji-Garmaroudi, S. Cacovich, C. Stavrakas, B. Philippe, J. M. Richter, M. Alsari, E. P. Booker, E. M. Hutter, A. J. Pearson, S. Lilliu, T. J. Savenije, H. Rensmo, G. Divitini, C. Ducati, R. H. Friend and S. D. Stranks, *Nature*, 2018, **555**, 497–501.
18 X. Dong, H. Hu, B. Lin, J. Ding and N. Yuan, *Chem. Commun.*, 2014, **50**, 14405–14408.
19 C. Y. Chang, K. T. Lee, W. K. Huang, H. Y. Siao and Y. C. Chang, *Chem. Mater.*, 2015, **27**, 5122–5130.
20 A. Hultqvist, K. Aitola, K. Sveinbjörnsson, Z. Saki, F. Larsson, T. Törndahl, E. Johansson, G. Boschloo and M. Edoff, *ACS Appl. Mater. Interfaces*, 2017, **9**, 29707–29716.
21 H. Si, Q. Liao, Z. Zhang, Y. Li, X. Yang, G. Zhang, Z. Kang and Y. Zhang, *Nano Energy*, 2016, **22**, 223–231.
22 D. Koushik, W. J. H. Verhees, D. Zhang, Y. Kuang, S. Veenstra, M. Creatore and R. E. I. Schropp, *Adv. Mater. Interfaces*, , DOI:10.1002/admi.201700043.
23 D. Koushik, W. J. H. Verhees, Y. Kuang, S. Veenstra, D. Zhang, M. A. Verheijen, M. Creatore and R. E. I. Schropp, *Energy Environ. Sci.*, 2017, **10**, 91–100.
24 M. Kot, C. Das, Z. Wang, K. Henkel, Z. Rouissi, K. Wojciechowski, H. J. Snaith and D. Schmeisser, *ChemSusChem*, 2016, **9**, 3401–3406.
25 G. W. P. Adhyaksa, L. W. Veldhuizen, Y. Kuang, S. Brittman, R. E. I. Schropp and E. C. Garnett, *Chem. Mater.*, 2016, **28**, 5259–5263.
26 X. Dong, X. Fang, M. Lv, B. Lin, S. Zhang, J. Ding and N. Yuan, *J. Mater. Chem. A*, 2015, **3**, 5360–5367.
27 V. Zardetto, B. L. Williams, A. Perrotta, F. Di Giacomo, M. A. Verheijen, R. Andriessen, W. M. M. Kessels and M. Creatore, *Sustain. Energy Fuels*, 2017, **1**, 30–55.
28 Y. Li, F. Qian, J. Xiang and C. M. Lieber, *Mater. Today*, 2006, **9**, 18–27.
29 E. C. Garnett, M. L. Brongersma, Y. Cui and M. D. McGehee, *Annu. Rev. Mater. Res.*, 2011, **41**, 269–295.

Formatted: German (Germany)

Formatted: Dutch (Netherlands)

Formatted: Dutch (Netherlands)

30 L. Cao, J. S. White, J.-S. Park, J. A. Schuller, B. M. Clemens and M. L. Brongersma, *Nat. Mater.*, 2009, **8**, 643–647.

31 F. Léonard, A. A. Talin, B. S. Swartzentruber and S. T. Picraux, 2009, **106805**, 1–4.

32 O. Demichel, V. Calvo, A. Besson, P. Noé, B. Salem, N. Pauc, F. Oehler, P. Gentile and N. Magnea, *Nano Lett.*, 2010, **10**, 2323–2329.

33 Y. Dan, K. Seo, K. Takei, J. H. Meza, A. Javey and K. B. Crozier, *Nano Lett.*, 2011, **11**, 2527–2532.

34 H. J. Joyce, J. Wong-Leung, C. K. Yong, C. J. Docherty, S. Paiman, Q. Gao, H. H. Tan, C. Jagadish, J. Lloyd-Hughes, L. M. Herz and M. B. Johnston, *Nano Lett.*, 2012, **12**, 5325–5330.

35 E. Horváth, M. Spina, Z. Szekrényes, K. Kamarás, R. Gaal, D. Gachet and L. Forró, *Nano Lett.*, 2014, **14**, 6761–6766.

36 J. Xing, X. F. Liu, Q. Zhang, S. T. Ha, Y. W. Yuan, C. Shen, T. C. Sum and Q. Xiong, *Nano Lett.*, 2015, **15**, 4571–4577.

37 M. M. Tavakoli, A. Waleed, L. Gu, D. Zhang, R. Tavakoli, B. Lei, W. Su, F. Fang and Z. Fan, *Nanoscale*, 2017, **9**, 5828–5834.

38 M. M. Tavakoli, K.-H. Tsui, S.-F. Leung, Q. Zhang, J. He, Y. Yao, D. Li and Z. Fan, *ACS Nano*, 2015, 150818123917002.

39 A. Waleed, M. M. Tavakoli, L. Gu, Z. Wang, D. Zhang, A. Manikandan, Q. Zhang, R.-J. Zhang, Y.-L. Chueh and Z. Fan, *Nano Lett.*, 2017, **17**, 523–530.

40 L. Gu, M. M. Tavakoli, D. Zhang, Q. Zhang, A. Waleed, Y. Xiao, K.-H. Tsui, Y. Lin, L. Liao, J. Wang and Z. Fan, *Adv. Mater.*, 2016, **28**, 9713–9721.

41 S. Z. Oener, P. Khoram, S. Brittman, S. A. Mann, Q. Zhang, Z. Fan, S. W. Boettcher and E. C. Garnett, *Nano Lett.*, 2017, **17**, 6557–6563.

42 Y. Yang, Y. Yan, M. Yang, S. Choi, K. Zhu, J. M. Luther and M. C. Beard, *Nat. Commun.*, 2015, **6**, 7961.

43 Y. Fang, Q. Dong, Y. Shao, Y. Yuan and J. Huang, *Nat. Photonics*.

44 B. Wu, H. T. Nguyen, Z. Ku, G. Han, D. Giovanni, N. Mathews, H. J. Fan and T. C. Sum, *Adv. Energy Mater.*, 2016, **6**, 1–9.

45 L. M. Herz, *Annu. Rev. Phys. Chem.*, 2016, **67**, 65–89.

46 Y. Yang, M. Yang, Z. Li, R. Crisp, K. Zhu and M. C. Beard, *J. Phys. Chem. Lett.*, 2015, **6**, 4688–4692.

47 J. M. Richter, M. Abdi-Jalebi, A. Sadhanala, M. Tabachnyk, J. P. H. Rivett, L. M. Pazos-Outón, K. C. Gödel, M. Price, F. Deschler and R. H. Friend, *Nat. Commun.*, 2016, **7**, 13941.

48 H. Wei, Y. Fang, P. Mulligan, W. Chuirazzi, H.-H. Fang, C. Wang, B. R. Ecker, Y. Gao, M. A. Loi, L. Cao and J. Huang, *Nat. Photonics*.

49 W. Yang, Y. Yao and C.-Q. Wu, *J. Appl. Phys.*, 2015, **117**, 155504.

50 H.-H. Fang, S. Adjokatse, H. Wei, J. Yang, G. R. Blake, J. Huang, J. Even and M. A. Loi, *Sci. Adv.*, 2016, **2**, e1600534–e1600534.

51 G. W. P. Adhyaksa, S. Brittman, Ā. Haralds, A. Lof, X. Li, T. Duevski, D. P. Fenning and E. C. Garnett, .

52 H.-H. Fang, R. Raissa, M. Abdu-Aguye, S. Adjokatse, G. R. Blake, J. Even and M. A. Loi, *Adv. Funct. Mater.*, 2015, **25**, n/a-n/a.